



# Graphene-based hybrid plasmonic optical electro-absorption modulator on InP platform

Hamid Nezamdoost<sup>1</sup> · Mahmoud Nikoufard<sup>2</sup> · Hamed Saghaei<sup>3,4</sup>

Received: 25 September 2023 / Accepted: 18 December 2023 / Published online: 27 January 2024  
© The Author(s), under exclusive licence to Springer Science+Business Media, LLC, part of Springer Nature 2024

## Abstract

This paper presents a novel design of an optical electro-absorption modulator based on a hybrid plasmonic structure with a graphene layer on the generic InP platform. Graphene-based optical modulators have the potential to revolutionize the field of optical communications. They enable high-speed data transfer and facilitate advancements in quantum computing. Developing a highly compact modulator on the InP platform represents a significant objective for photonics researchers aiming to achieve large-scale photonic integration technology. In the proposed design, a metal layer on top of a ridge waveguide creates a hybrid plasmonic structure. At the same time, light modulation is accomplished by applying a bias voltage to the graphene layer. By manipulating the optical absorption properties through changes in the Fermi level of the graphene layer, calculations demonstrate a 3 dB bandwidth exceeding 70 GHz at  $\lambda = 1.55 \mu\text{m}$  for a  $1 \mu\text{m}$  length. Furthermore, the impact of metal and  $\text{SiO}_2$  dielectric layer thicknesses and chemical potential on the real part of the effective index, optical absorption, 3 dB bandwidth, extinction ratio, and insertion loss are quantitatively determined.

**Keywords** Graphene · Electro-absorption · Modulator · Hybrid plasmonic · InP platform

## 1 Introduction

Optical communication development relies heavily on optical modulators, which have experienced significant advancements in recent years; for instance, their bandwidth has increased from a few megahertz to several gigahertz within three decades. To optimize the performance of modulators, it is crucial to minimize device size and energy consumption

---

✉ Mahmoud Nikoufard  
mnik@kashanu.ac.ir

<sup>1</sup> Nanoscience and Nanotechnology Research Center, University of Kashan, Kashan, Iran

<sup>2</sup> Department of Electronics, Faculty of Electrical and Computer Engineering, University of Kashan, Kashan, Iran

<sup>3</sup> Department of Electrical Engineering, Shahrekord Branch, Islamic Azad University, Shahrekord, Iran

<sup>4</sup> Energy Research Center, Shahrekord Branch, Islamic Azad University, Shahrekord, Iran

while increasing bandwidth and ER within the acceptable operating temperature and optical spectral width ranges (Reed et al. 2010; Lee et al. 2010; Liu et al. 2004; Xu et al. 2005; Bogaerts et al. 2011; Rezaei and Zarifkar 2019; Baqir et al. 2021). Graphene offers exceptional electro-optic properties that make it ideal for use in optical modulators. Its ability to support surface plasmon polaritons (SPPs) makes it attractive for compact and high-speed devices (Koester and Li 2014; Ando et al. 2013; Bao and Loh 2012; Liu et al. 2011; Rezaei and Zarifkar 2018). By achieving these goals, graphene-based optical modulators hold the potential to revolutionize the field of optical communications and enable new applications such as high-speed data transfer and quantum computing (Calafell et al. 2019). Graphene-based modulators are increasingly being integrated into silicon photonic (SOI) platforms (Shu et al. 2018; Bonaccorso et al. 2010; Rezaei and Shiri 2021). This integration enables the development of high-performance and low-power optical communication systems (Naghizade and Saghaei 2020, 2021a, 2021b, 2021c, 2022; Naghizade et al. 2022, 2023; Alden Mostaan and Saghaei 2021; Nayyeri Raad et al. 2023; Rezaei et al. 2018, 2019, 2020). The combination of graphene's exceptional electro-optic properties and SOI's compatibility with existing semiconductor technology provides numerous advantages for optical modulators. These include the ability to operate at high speeds and frequencies, low IL, and efficient energy use. Additionally, using SOI platforms allows for incorporating other passive components, such as optical filters and couplers, leading to more compact and efficient systems. However, it has an indirect bandgap and lacks lasing at 1550 nm optical communication wavelength. Meanwhile, the InP-based photonic platform can perform all photonic operations with a medium gain. The InP-based modulator on a conventional platform has a length of a few hundred micrometers. Thus, the design of a very compact modulator on the InP platform could be a great goal for photonic researchers to reach very large-scale photonic integration technology. Optical modulators change light properties, such as phase, amplitude, and polarization, by thermo-optical (Sirleto et al. 2010), electro-optics (Soref and Bennett 1987), and electro-absorption modulation techniques (Thomson et al. 2010; Didari-Bader and Saghaei 2023). These modulators are usually based on Mach-Zehnder interferometer (MZIs) (Dereux et al. 2012), ring resonators (RRs) (Dereux et al. 2010) and electro-absorption (EA) (Bijlani et al. 1550) configurations. To overcome the size limitations of various modulator schemes, the unique electrooptical properties of graphene can be utilized (Novoselov et al. 2005; Vakil and Engheta 1979). Various structures of EAMs have been proposed, where the electrooptical properties of a graphene sheet are changed by applying a voltage and performing light modulation (Liu et al. 2011, 2012).

The researchers present a distinctive design featuring a thermally/electrically tunable polarizer (Farmani et al. 2017; Hamzavi-Zarghani et al. 2019; Baqir et al. 2019). To achieve this, a multilayer graphene, known for its adjustable optical properties, is employed on a hexagonal boron-nitride substrate, often referred to as white graphene. This innovative approach results in the creation of a polarizer capable of manipulating the polarization of reflected light within the near-infrared (NIR) range (Emaminejad et al. 2021; Baqir et al. 2018). Also, to increase the effect of optical absorption, the graphene sheet is placed where the electric field is maximum (Liu et al. 2012). Liu et al. (2011) fabricated a graphene modulator based on silicon with a length of 60  $\mu\text{m}$  and a bandwidth of 1.2 GHz (Liu et al. 2011). Lu and Zhao (2012) simulated a modulator structure consisting of a layer of graphene sandwiched between two dielectric layers. They found that this structure could achieve an ER of 3 dB over a length of 800 nm for a silicon waveguide and 120 nm for a plasmonic waveguide. This configuration offers several advantages, including small size, low loss, low power consumption, and high bandwidth (Lu and Zhao 2012). Koester et al. (2012) proposed a design of a bilayer graphene, with a dielectric layer in between,

that has an ER of 0.5 dB and a bandwidth of 120 GHz, with a length of 60  $\mu\text{m}$  (Koester and Li 2012). Gosciniak et al. (2013a; b) presented optical modulators based on bilayer graphene with a length of 600 nm and a modulation speed of 160–850 GHz on a silicon substrate (Gosciniak and Tan 2013a). In order to increase the interaction of graphene with the propagating light in the waveguide, Ye et al. (2014) proposed a different structure from the others using bilayer graphene, which not only reduces the length of the modulator but also increases the ER to 34 dB and achieves a bandwidth of 100 GHz (Ye et al. 2014). However, their structure is challenging from the fabrication point of view. Furthermore, Ansell et al. (2015) have proposed a plasmonic modulator, which has a flat structure with a size of 10  $\mu\text{m}^2$  and an ER of at least 0.03 dB/ $\mu\text{m}$ , using a completely different structure from the waveguide mentioned earlier (Ansell et al. 2015). Hu et al. (2016) have suggested and fabricated a high-speed electro-absorption modulator by optimizing the design and fabrication processes, which has an insertion loss (IL) of 3.8 dB and an ER of 2.5 dB while reducing the series resistance to 241  $\Omega$  and the capacitance to 80 fF. The modulation speed of 10 Gb/s and 3-dB bandwidth of 5.8 GHz has been achieved, and the power consumption per bit has been calculated as 350 fJ/bit (Hu et al. 2016). In 2019, Giambra et al. developed a high-speed modulator with a length of 120  $\mu\text{m}$  and ER of 0.137 dB/ $\mu\text{m}$ . They used a combination of gold and nickel to reduce the series resistance, bringing the value to less than 10  $\Omega$ , with a capacitance of 204 fF. They achieved a remarkable 3-dB bandwidth of 29 GHz and ER of 1.3 dB at 50 Gb/s (Giambra et al. 2019). To increase the effect of optical absorption, plasmonic waveguides such as dielectric-loaded surface plasmon polariton waveguides (DLSPPWs) were proposed, whose important features are very strong mode confinement, low IL and easy connection to control electrodes. One of the advantages of plasmonic modulators is that the noble metal (e.g., Ag or Au) can be used simultaneously to apply voltage. This can also provide another opportunity to integrate optics and electronics (Holmgaard and Bozhevolnyi 2007; Ebbesen et al. 2008). Although silicon substrates are compatible with CMOS manufacturing methods and allow passive devices to be built, platforms such as InP must be used to integrate lasers, LEDs, and modulators monolithically. This can reduce manufacturing costs and solve some integration challenges. InP platform gains several benefits concerning its rivals, mainly monolithic integration of passive and active devices (such as laser, semiconductor optical amplifier, photodetector, and modulator) (Smit et al. 2019). However, there are no reports on graphene-based devices on the InP platform. The production of graphene for practical applications encompasses various established methods. Mechanical exfoliation, pioneered by Novoselov and colleagues, involves the layer-by-layer separation of graphene from graphite using an adhesive technique, producing high-quality graphene, albeit unsuitable for large-scale production (Geim and Novoselov 2007). Alternatively, chemical vapor deposition (CVD) is widely utilized, wherein graphene is grown on a copper substrate using carbon-containing gases like methane, resulting in high-quality graphene amenable to large-scale production (Pizzocchero et al. 2022). Liquid phase exfoliation employs ultrasonic treatment on graphite placed in a solution to break down bulk graphite into graphene flakes, yielding liquid-phase graphene ideal for layer deposition (Sellathurai et al. 2023). Another technique, Epitaxial growth, involves growing a graphene layer on a silicon carbide (SiC) substrate, generating high-quality graphene albeit limited to specific substrates (Huang et al. 2014). Additionally, the plasma-enhanced chemical vapor deposition method combines elements of CVD and plasma techniques, simplifying the production and enabling precise control of graphene characteristics (Woehrl et al. 2014). The selection of a specific method depends on the intended application and required scale. Depending on the unique needs, a combination of these methods can be employed to produce the desired high-quality graphene, emphasizing

the adaptability of graphene synthesis methods to diverse research contexts. Khajeh et al. (2021) proposed two optimization algorithms to design broadband polarization converters based on coded metasurfaces. A pixelated graphene patch with an elliptic structure was proposed for the initial solution, where each pixel represented the presence (1) or absence (0) of graphene. By changing the chemical potential of graphene, the operation frequency of the polarization converters could be adjusted (Khajeh et al. 2021).

This article focuses on an EA-modulator on a hybrid plasmonic InP-based platform (Soleimannezhad et al. 2020) at the 1.55  $\mu\text{m}$  communication wavelength. We investigated an EA-modulator on a hybrid plasmonic waveguide with a three-layer of graphene for the first time. The proposed EAM uses an InP-based platform, which can be monolithic and integrated with passive and active photonic devices. The proposed structure offers the advantage of having a short length of only a few micrometers, which is comparable to the length of its counterpart in the InP generic platform, which typically requires a few hundred micrometers in length. The proposed structure will be introduced in the following section, after which various device parameters will be determined. These parameters include the real part of the refractive index, optical absorption, IL, extinction ratio (ER), and 3-dB bandwidth. During the optimization process, the thicknesses of the gold and  $\text{SiO}_2$  layers will be varied to determine the optimum values. In contrast, the thickness of the remaining layers will be kept constant using the generic InP platform.

## 2 The proposed modulator

In our research, Benzocyclobutene (BCB) emerged as a key component due to its widespread application as a photosensitive polymer in microelectromechanical systems (MEMS) and microelectronics processes. BCB-based polymer dielectrics are commonly employed as coatings on various substrates, utilizing advanced spin-coating techniques. One of the remarkable attributes of BCB is its role in planarizing structures during the fabrication process, providing a smooth surface conducive to subsequent graphene layer deposition. This quality proves invaluable in the proposed design of the ridge waveguide, where BCB was strategically chosen to ensure optimal planarization of the waveguide surface. Moreover, the precise refractive index of the BCB structure, crucial for our simulations, was meticulously determined to be 1.54. The proposed EA-modulator, depicted in Fig. 1, comprises a deeply etched passive waveguide based on the generic InP platform. The waveguide includes an InGaAsP layer with a bandgap wavelength of 1.25  $\mu\text{m}$  and a thickness of 500 nm on an InP substrate. Soleimannezhad et al. (2020) proposed the design of an InP-based hybrid plasmonic waveguide (HPWG). The proposed HPWG demonstrated an impressive propagation length of at least 100  $\mu\text{m}$  for a 100 nm waveguide ridge width—twice the propagation length of a comparable silicon-on-insulator (SOI)-based HPWG. This structural advancement is compatible with the generic InP-based layer stack and is well-suited for monolithic integration with active devices, such as lasers and photodetectors, operating at a wavelength of 1.55  $\mu\text{m}$  (Soleimannezhad et al. 2020). Building upon the insights presented by Soleimannezhad et al. in their discussion of the plasmonic waveguide platform, our study is dedicated to achieving a seamless collaboration with the InP platform.

Here, the three graphene layers, with a thickness of 1.12 nm, were deposited onto the waveguide. Figure 1 illustrates the positioning of the graphene layer beneath the metal contact, which in turn is situated under the  $\text{SiO}_2$ -clad layer. The part of the graphene that is

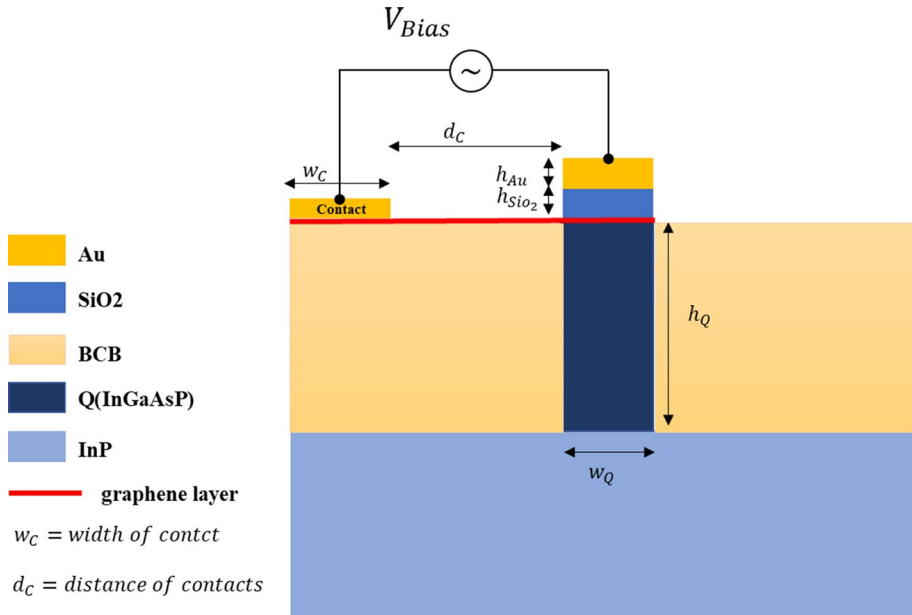


**Fig. 1** Cross-sectional view of the proposed modulator on the InP-based platform

under the SiO<sub>2</sub> layer acts as the graphene modulator. In fact, the second electrode on the ridge region is placed for two purposes: first, to create plasmonic effects to concentrate light under the metal layer and propagate light in the SiO<sub>2</sub> layer, and second, to make a metallic connection to the power supply or pulse generator to send information on the modulator to create changes in the electro-optic properties of the graphene layer and perform optical modulation. A thin layer of SiO<sub>2</sub> with a thickness of 20 nm is then added, which is capped with a layer of gold (Au) with a thickness of 100 nm. This plasmonic structure is used to enhance the performance of the modulator. The thickness of the gold (Au) layer is enough to excite plasmon polaritons, a phenomenon where light and electrons oscillate together on the surface of the metal. As a result, we anticipate that the majority of the optical power will be focused on the low-index material of the SiO<sub>2</sub> layer and, to some extent, on the graphene layer (Soleimannezhad et al. 2020). From the other point of view, the proposed structure resembles a capacitor, with SiO<sub>2</sub> as the dielectric material. The application of voltage to the electrodes generates an electric field above the graphene layer, altering charge accumulation on the graphene. Equation (1) shows how surface charge  $n_s$  on the graphene is related to the capacitance of the  $C_{ox}$  and  $V_{Bias}$ . This charge accumulation, in conjunction with changes in charge distribution within the graphene layer (see Eq. 2), which relates the chemical potential to surface charge density  $n_s$ , ultimately closed form solution of Eqs. (1) and (2), leads to Eq. (3), which connects the Fermi level or chemical potential of the graphene to the Bias voltage applied to the electrodes (see Eq. 3). Based on the Kubo formula (see Eq. 4), this results in alterations of conductivity and permittivity of graphene.

$$C_{ox} V_{Bias} = q_e n_s \quad (1)$$

$$n_s = \frac{2}{\pi \hbar^2 v_f^2} \int_0^\infty \epsilon [f_d(\epsilon - \mu_c) - f_d(\epsilon + \mu_c)] \partial \epsilon \tag{2}$$

$$\mu_c \approx \hbar v_f \sqrt{\frac{\pi C_{ox} V_{Bias}}{q}} \tag{3}$$

An electric field will be applied to the graphene layer by using an electrode on top of the graphene layer with a  $d_c$  distance from the modulator ridge. The applied voltage of  $V_{bias}$  varies the chemical potential of graphene, changing the real and imaginary parts of the refractive index of graphene. In this way, it is possible to have two modulator types: we can obtain an EAM by a butt coupling of the proposed structure to a plasmonic waveguide proposed in ref. (Soleimannezhad et al. 2020; Nikoufard et al. 2017) or a conventional InP-based passive waveguide (Soleimannezhad et al. 2020), or reach an EOM by using the proposed structure in an arm of the Mach-Zehnder interferometer (MZI) (Thomson et al. 2010).

In the first type, which is the main goal of this article, the imaginary part of the graphene refractive index should be switched between two low and high levels to turn off and on the EAM. In an on-state, the incident optical power to the input facet of EAM absorbs within the graphene layer, and the optical power will mainly be diminished in the output facet; in contrast, in the off-state, it will mostly emerge. The refractive index of InP, InGaAsP(1.25), SiO<sub>2</sub>, BCB, and Au are, respectively, 3.17, 3.367, 1.44, 1.54, 0.524 + 10.472i. The refractive index of graphene can be determined as follows:

$$\sigma(\omega) = \underbrace{\frac{\sigma_0}{2} \left( \tanh \frac{\hbar\omega + 2\mu}{4K_B T} + \tanh \frac{\hbar\omega - 2\mu}{4K_B T} \right)}_{\text{interband}} - i \underbrace{\frac{\sigma_0}{2} \log \left( \frac{(\hbar\omega + 2\mu)^2}{(\hbar\omega - 2\mu)^2 + (2K_B T)^2} \right)}_{\text{interband}} + i \underbrace{\frac{4\sigma_0}{\pi} \frac{\mu}{\hbar\omega + i\hbar\gamma}}_{\text{interband}} \tag{4}$$

$$\epsilon(\omega) = 1 + \frac{\sigma_{total}(\omega)}{\omega \epsilon_0 d} \tag{5}$$

where  $\sigma_{total}(\omega)$  is the conductivity of graphene,  $\mu$  is the Fermi level of graphene,  $\omega$  is the optical frequency,  $\gamma = 54\text{meV}$  is the inter-band dispersion rate,  $h$  is the Planck’s constant,  $e$  is the electron charge,  $\sigma_0 = e^2 / 4\hbar \cong 60.8 \mu\text{s}$  is the global constant of conductivity,  $K_B$  is the Boltzmann’s constant,  $T$  is the temperature in Kelvin,  $\epsilon$  is the permittivity, and  $n$  is the refractive index of graphene.

The conductivity Eq. (4),  $\sigma(\omega)$ , has been obtained from Kubo’s formula,  $\epsilon_1$  and  $\epsilon_2$  show the real and imaginary parts of  $\epsilon(\omega)$  obtained from Eq. (5). Parameters of angular frequency ( $\omega$ ), chemical potential ( $\mu$ ), dispersion rate ( $\gamma$ ), and temperature ( $T$ ) affect the conductivity and then the transmittance at different voltage levels (Gosciniak and Tan 2013a, b; Ye et al. 2014; Fan et al. 2017; Hao et al. 2013). The real and imaginary parts of the refractive index of three graphene layers at an optical communication wavelength

of 1.55  $\mu\text{m}$  and temperature of 300 K within the chemical potential range of 0–1 eV were determined using Eqs. (4), (5) and plotted in Fig. 2.

In graphene material, changes to the chemical potential within the 0.4–0.6 eV range result in significant changes to the real and imaginary parts of the permittivity and consequently refractive index. Specifically, within this range, the real component of the permittivity decreases while the real component takes on negative values. Graphene's properties transition from dielectric to metallic within the above chemical potential range. Moreover, the real part of the refractive index exhibits a maximum value at a chemical potential of 0.4 eV, followed by a steep decline. The real part of  $\epsilon$  becomes negative after the chemical potential of  $\mu = 0.525$  eV. When the real part of  $\epsilon$  becomes nearly zero, this effect is called the epsilon near zero (ENZ) effect, i.e.,  $\epsilon(0.525 \text{ eV}) = -0.0179 + 0.32i$ . So that, at this chemical potential, TM mode loss is maximized. The presence of the ENZ effect leads to a rapid decrease in the amplitude of the fundamental TM mode (Koester and Li 2014, 2012; Hu et al. 2016). To investigate the impact on propagating light at the optical communication wavelength of 1550 nm, we examine two specific chemical potentials of 0.4 eV and 0.525 eV, which are known to have a significant effect. At these chemical potentials, the refractive indices of graphene are  $n(0.4 \text{ eV}) = 1.95 + 0.7i$  and  $n(0.525 \text{ eV}) = 0.39 + 0.41i$ .

### 3 Simulation results

The real part of the refractive index of the structure is determined as a function of ridge width shown in Fig. 3. If the ridge width is increased beyond 400 nm, more modes will emerge. Therefore, to ensure that only the fundamental transverse magnetic (TM) mode propagates, the ridge width should be kept below 400 nm. The electrical field distribution (norm and direction) of the proposed structure has been illustrated in Figs. 4 and 5, respectively, for the two states of on and off. The on and off states correspond to chemical potentials of 0.4 and 0.525 eV, respectively. This structure supports the fundamental transverse magnetic (TM) modes for a ridge width of 100 nm with effective refractive indices of 1.848–0.0089i and 1.85–0.062i for on and off states, respectively. The behavior of the real part of the effective index is closely related to the refractive index of the  $\text{SiO}_2$  and  $\text{InP/}$

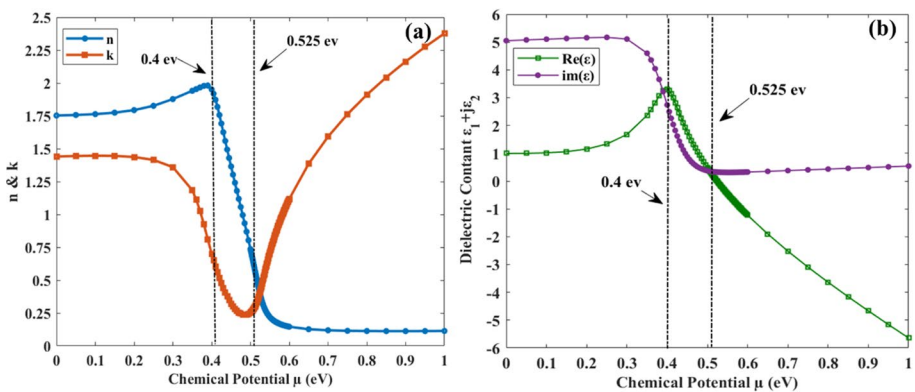


**Fig. 2** a The real and imaginary part of the graphene refractive index b The real and imaginary part of the graphene permittivity as a function of chemical potential ( $T = 300$  K,  $\lambda = 1550$  nm)

**Fig. 3** The real part of the effective refractive index of TM modes versus waveguide ridge width

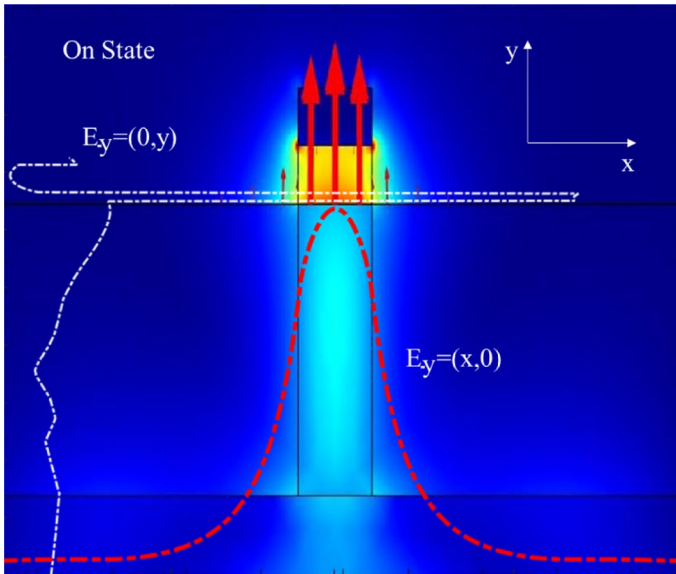
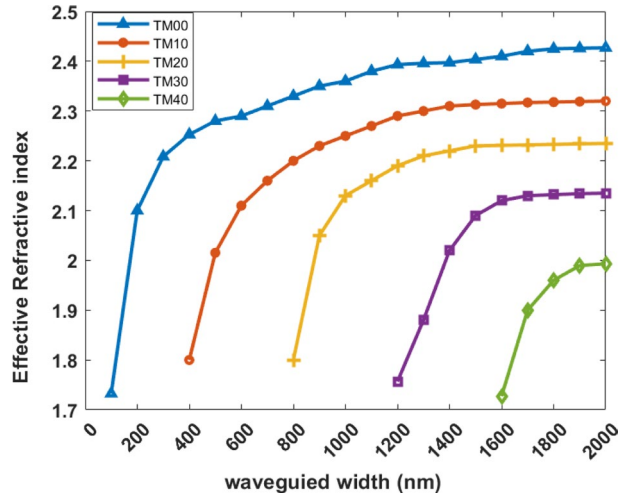


**Fig. 4** The 2D distribution of the TM mode’s electrical field (norm and direction) when the modulator is on-state. The 1D distribution of the electrical field norm is shown by the dashed line in the middle of the ridge width (y-direction) and inside the SiO<sub>2</sub> layer (x-direction)

InGaAsP materials. However, applying a voltage to the graphene layer has a negligible effect on the real part of the effective index. In contrast, the applied voltage significantly affects the imaginary part of the effective index. The mode profiles and effective indices were accurately determined utilizing the finite element method (FEM) with a tailored mesh configuration optimized for both graphene and SiO<sub>2</sub> layers. Even though light confinement within the structure was ensured, perfectly matched layer boundary conditions were applied to minimize undesirable reflections from the boundaries. This meticulous approach



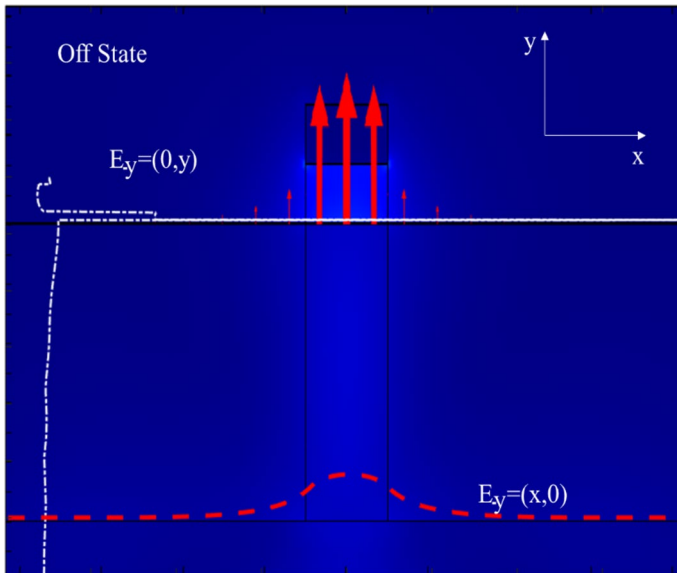


**Fig. 5** The 2D distribution of the TM mode's electrical field (norm and direction) when the modulator is off-state. The 1D distribution of the electrical field (norm) is shown by the dashed line in the middle of the ridge width (y-direction) and inside the SiO<sub>2</sub> layer (x-direction)

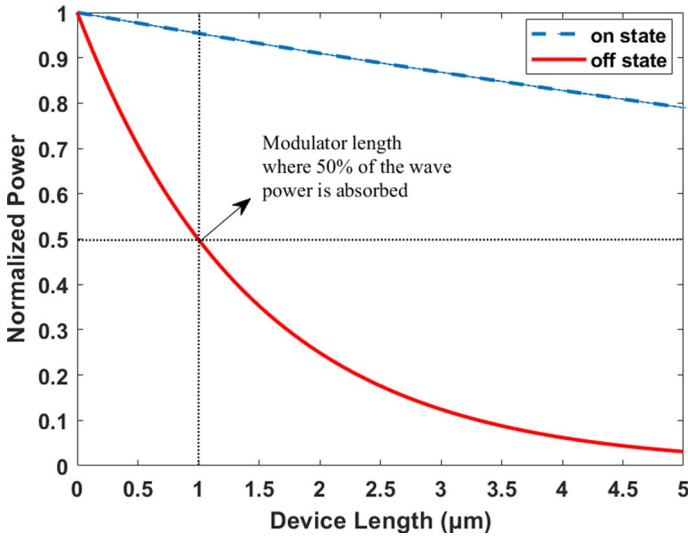
allowed us to precisely analyze the behavior of light within the graphene and SiO<sub>2</sub> layers, ensuring the integrity and accuracy of our results. In both the on and off states, the SiO<sub>2</sub> layer has a greater impact on the real part of the refractive index than the other layers. This is because the optical field is more concentrated in the SiO<sub>2</sub> layer, which serves as the guiding layer.

Figure 4 shows that the optical fields are mainly concentrated in the SiO<sub>2</sub> layer as a property of plasmonic structures while the EAM is in the on state ( $\mu_c = 0.4$  eV). By changing the chemical potential of graphene to 0.525 eV (off state), the optical field will be dramatically focused and absorbed on the graphene layer (see Fig. 5). At the same time, the imaginary part of the effective index of the EAM structure becomes an order higher than respect to off state situation, the imaginary part of the effective index varies from 0.009 to 0.063.

Setting the chemical potential to 0.525 eV increases the absorption coefficient of graphene to its maximum value, resulting in the electrical field within the graphene layer reaching its maximum value. In contrast, the electrical field within the oxide layer decreases. We can modulate the incident light by tuning the applied voltage to the graphene.

Figure 6 shows the propagation of the norm of the electrical field inside the SiO<sub>2</sub> layer in two states of on and off. The magnitude of the electrical field exponentially decays due to two lossy materials, Au and graphene.

In this study, the appropriate selection of important parameters such as IL, ER, and bandwidth, is crucial for optimizing the design of the optical modulator. The rationale underlying our choice of these parameters is deeply grounded in their significant impact on various facets of optical communication system performance. Foremost, our emphasis on minimizing IL is driven by its important role in maintaining signal strength, ensuring reliable transmission, and enhancing overall system efficiency. This becomes particularly

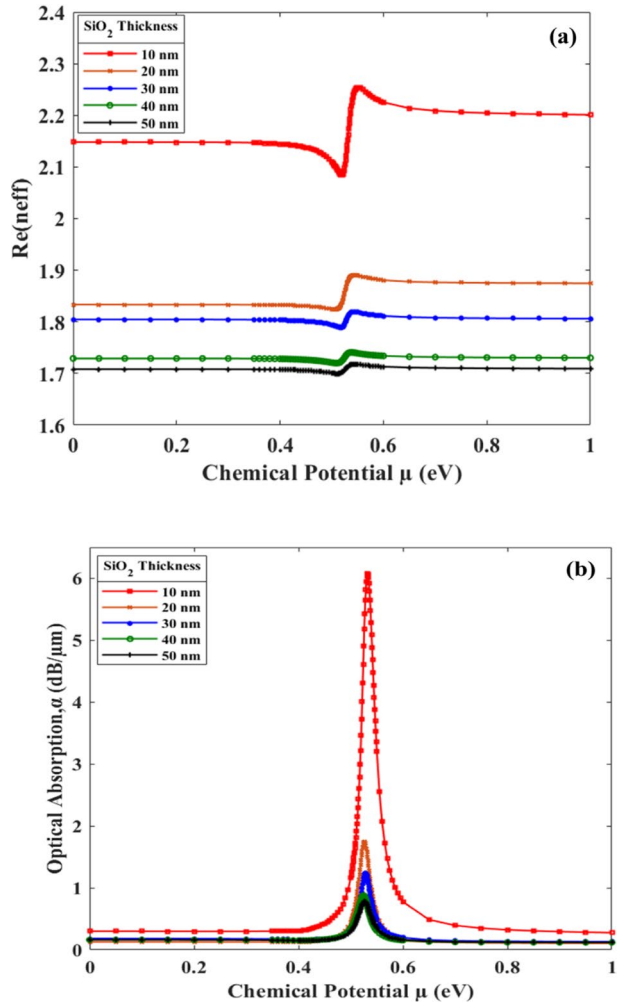


**Fig. 6** The normalized magnitude of the propagated electrical field inside the SiO<sub>2</sub> layer in on and off states

crucial in long-distance optical communication scenarios, where the reduction of power requirements and the necessity for additional amplification stages are paramount. Additionally, our consideration of extinction ratio involves meticulous calculations to enhance the signal-to-noise ratio, data integrity, receiver sensitivity, and dynamic range. Lastly, the careful selection of bandwidth is imperative to enable higher data rates, support high-speed communication, ensure compatibility with transmission systems, and facilitate the precise and accurate transmission of modulated signals. Considering the crucial parameters mentioned above, our focus will be on studying and optimizing these factors. In the off-state, the electrical field will diminish within a few micrometers. In order to determine the 3 dB-bandwidth, *ER* and *IL* parameters, it is essential to calculate the modulator length required for switching between the on and off states.

To determine this length, the stance that the electrical field propagates along the SiO<sub>2</sub> guiding layer in the off state to reach 50% of its initial power value is considered, as described in Reed et al. (2010). Using the FEM method, it has been observed that the power of the electrical field drops to 50% within a length of 1 μm, as shown in Fig. 6. Since the SiO<sub>2</sub> guiding layer plays the main role in the proposed EAM, the effect of the SiO<sub>2</sub> layer thickness on the effective index and optical absorption ( $\alpha = \lambda \text{Im}(n_{\text{eff}})/4\pi$ ) in the range of chemical potentials of 0–1 eV is determined (see Fig. 7). For a SiO<sub>2</sub> layer thickness of 10 nm, the effective index and optical absorption exhibit notable variations in their real part, with a dip observed at 0.4 eV and a peak at 0.525 eV for chemical potentials ranging from 0.4 to 0.6 eV. However, these changes are suppressed for other chemical potential values due to the refractive index of the graphene layer. In the spectral range below 0.4 eV and above 0.6 eV, the behavior exhibits similarity: the real effective index remains relatively constant, and absorption is negligible. This indicates that both the real effective index and absorption are minimally influenced by changes in the chemical potential within these two regions, emphasizing their weak dependency on the chemical potential. The strongest absorption is at 0.525 eV for a SiO<sub>2</sub> layer with a thickness of 10 nm and drops by increasing the thickness of the SiO<sub>2</sub> layer. These dips and peaks shift by increasing the SiO<sub>2</sub> layer

**Fig. 7** **a** The real part of effective refractive index **b** optical absorption versus chemical potential changes for different SiO<sub>2</sub> layer thicknesses



thickness. The concentration of the optical field inside both the SiO<sub>2</sub> layer and graphene layer directly affects the amount of optical absorption and the shift in the peaks, as well as the real and imaginary parts of the effective index. The real part of the effective index varies from 1.7 to 2.3, and absorption is in the range of 0.7–6 dB/μm by changing the SiO<sub>2</sub> layer thickness from 10 to 50 nm and chemical potential from 0–1 eV. Therefore, a thinner SiO<sub>2</sub> layer can impose a stronger effect on switching states, but other parameters, such as *IL* and propagation length, will be decisive in selecting SiO<sub>2</sub> layer thickness.

*IL* and *ER* were calculated using the imaginary part of the effective refractive index for on and off states of EAM at chemical potential values of 0.4 and 0.52 eV, respectively, as (Koester and Li 2014; Narayanan Mathivanan 2019):

$$IL = -10 \log_{10}(T_{\max}) = -10 \log_{10}(\exp^{-4\pi\alpha_{\text{on}}L}) \tag{6}$$

$$ER = 10 \log_{10} \left( \frac{T_{\max}}{T_{\min}} \right) = 10 \log_{10} \left( \frac{\exp^{-4\pi\alpha_{\text{on}}L}}{\exp^{-4\pi\alpha_{\text{off}}L}} \right) \tag{7}$$

Figure 8 shows the *IL* and *ER* as a function of the thickness of the SiO<sub>2</sub> layer. We defined the off-state in 0.4 eV and on-state in the 0.525 eV chemical potential whose absorption is in the peak value shown in Fig. 7b. For a thicker SiO<sub>2</sub> layer, the *IL* value changes sharply downward, tending to 0.2–0.3 dB/μm. This trend shows that increasing the SiO<sub>2</sub> thickness reduces the IL because less light is concentrated in the border of the Au layer. On the other hand, obtaining a high *ER* in optical modulators is desirable. Figure 8 shows that increasing the SiO<sub>2</sub> thickness from 10 to 50 nm decreases the *ER* from 9 dB to less than 1 dB, respectively. Therefore, there is a tradeoff between *IL* and *ER* in selecting SiO<sub>2</sub> layer thickness.

The effect of the gold metal layer thickness on the real part of the effective refractive index, light absorption, *IL*, and *ER* is also investigated at various chemical potentials applied on the graphene layer. The SiO<sub>2</sub> layer thickness was kept equal to 10 nm, and the gold layer thickness was increased from 5 to 50 nm. Increasing the gold layer thickness above 50 nm does not significantly change the real part of the effective index and optical absorption and overlaps with other curves, so we have not shown in Fig. 9. Figure 9a shows the real part of the effective index as a function of chemical potential for various Au layer thicknesses. Increasing the Au layer thickness decreases the real part of the effective index, and less light will be confined in the SiO<sub>2</sub> layer.

At a wavelength of 1550nm, the optical field penetrates approximately 24nm into the gold layer, based on the calculation  $\lambda/2\pi\text{Im}(n_{\text{eff}})$ . This penetration depth means the gold thickness must exceed 24nm in order to maintain the plasmonic behavior of the EAM and excite SPP modes. The optical absorption will be dramatically increased by decreasing the gold layer thickness. Because the optical field will be shifted toward the InGaAsP layer, the magnitude of the optical field inside the graphene layer will be

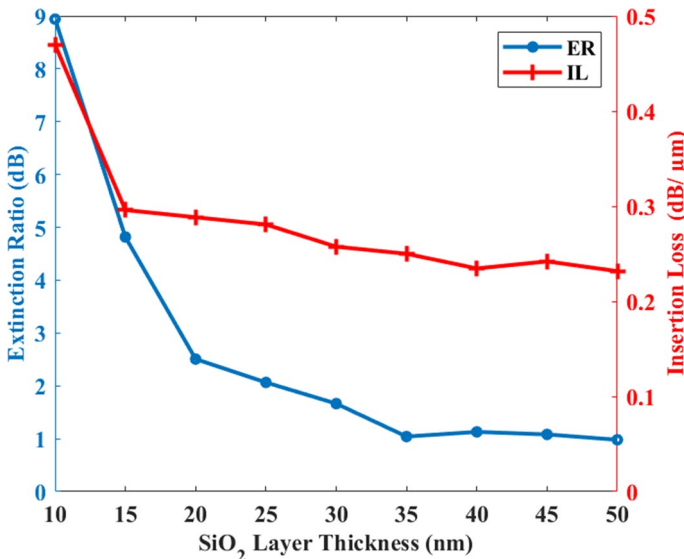
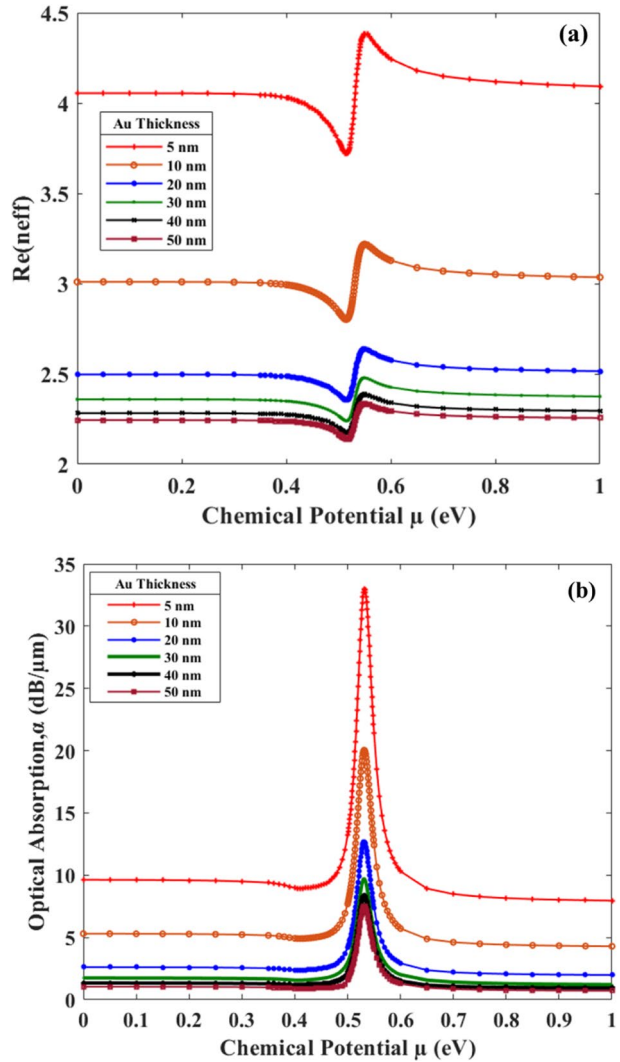


Fig. 8 Insertion loss and extinction ratio as a function of SiO<sub>2</sub> layer thicknesses for an EAM length of 1 μm

**Fig. 9** **a** Real part of the effective index **b** optical absorption as a function chemical potential for Au layer thickness of 5, 10, 20, 30, 40, 50 nm and SiO<sub>2</sub> layer thickness of 10 nm



increased. So, the optical absorption peaks increase from 6 to 33 dB/ $\mu\text{m}$  by reducing the Au layer thickness from 50 to 5 nm.

The effect of the gold layer thickness was studied on the *IL* and *ER*, shown in Fig. 10. Both parameters exponentially decay by increasing the gold layer thickness, in which the *IL* and *ER* have substantial reduction above the 50 nm thickness of the gold layer. A 5 nm-thick Au layer provided an *ER* of up to 35 dB, whereas increasing the Au layer thickness decreased *ER*, reaching less than 15 dB. This reduction can be attributed to a decline in the interaction between the optical field and the graphene layer as the gold thickness increases. A very important parameter in modulators is 3-dB bandwidth, which can be calculated as (Koester and Li 2012; Dawlaty et al. 2008):

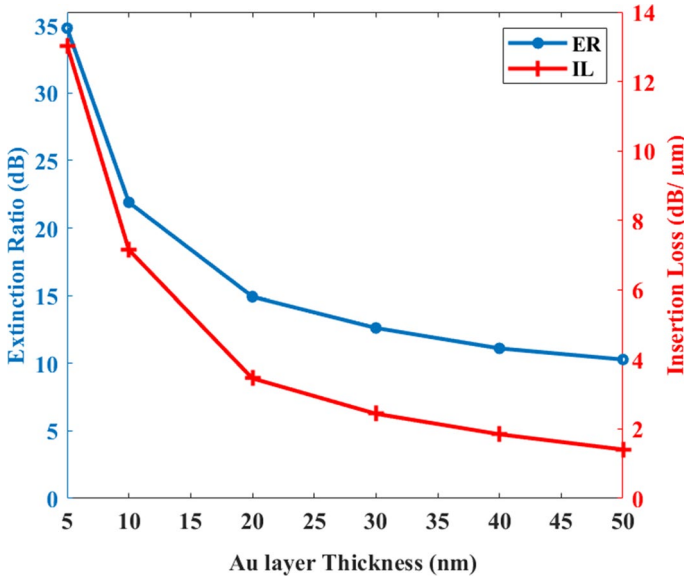


**Fig. 10** Insertion loss and extinction ratio as a function of the gold layer thickness for SiO2 layer thickness of 10nm and EAM length of 1 μm

$$f_{3dB} = \frac{1}{2\pi R_t C} \tag{8}$$

where  $R_t$  is the total resistance, which can be obtained as

$$R_t = R_c + R_g \tag{9}$$

$$R_g = \text{sheet Resistance of graphene} \times \frac{L_m}{\text{contact length}} \tag{10}$$

$$R_{\text{contact}} = \frac{\rho_c}{w_c} \tag{11}$$

$R_c$  and  $R_g$  are the contact and graphene resistances, respectively  $\rho_c$  is the contact resistance between the graphene and Au/Cr layers,  $w_c$  is the width of contact which is 100 nm,  $L_m$  is the modulator length. The connection of metal and graphene arises from the unique physical interaction between the metal connection and the graphene atomic layers (Dawlaty et al. 2008). The value of the metal and graphene junction resistance can change according to the metal type, the fabrication method, the amount of biasing voltage, and the measurement conditions (Xia et al. 2011; Giubileo and Bartolomeo 2017). According to experimental results, this value can vary from several hundred ohm-micrometers to several thousand ohm-micrometers (Peng et al. 2015; Xia et al. 2009). The value of contact resistance for Cr/Au contact is  $\rho_c = 3000 \Omega\text{m}$ , and the sheet resistance of graphene is  $1870 \Omega/\text{W}$  which is according to the dimensions of the device and also considering the following equivalent circuit.

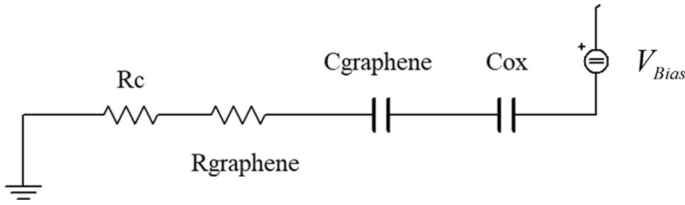
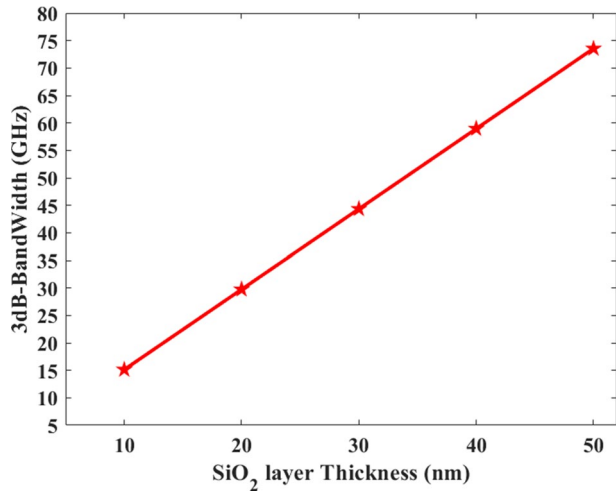


**Fig. 11** The equivalent circuit of the proposed EAM structure, which includes contact resistance between graphene and metal layers, graphene resistance, oxide capacitor, and graphene capacitor

**Fig. 12** Bandwidth of the modulator a versus SiO<sub>2</sub> thickness



Also, In Fig. 11, two capacitors,  $C_{\text{graphene}}$  and  $C_{\text{ox}}$ , are arranged in series.  $C_{\text{graphene}}$  corresponds to the graphene capacitor, while  $C_{\text{ox}}$  represents the silicon dioxide (SiO<sub>2</sub>) capacitor. Due to its extremely thin graphene layer, the graphene capacitor behaves as a quantum capacitor (Xia et al. 2009; Chen and Appenzeller 2008; Koester et al. 2012). The quantum capacitance value for three-layer graphene was calculated, and the capacitance value for the oxide layer was determined based on the thickness of the oxide. We calculated the bandwidth of the modulator in terms of different oxide thicknesses shown in Fig. 12. It can be seen that increasing the SiO<sub>2</sub> layer thickness will increase the bandwidth. The bandwidth value will increase the lower the resistance value and the capacitance value of the structure. Of course, although a large bandwidth is desirable, at the same time, the amount of bandwidth increase will also have limitations, including the limitation of the minimum resistance and capacitor of the structure. Using the sizes considered for the structure, as well as the materials used in the structure, the resistance value for the structure with Cr/Au connection (10/100 nm) has been calculated.

### 4 Conclusion

This study employed a three-layer graphene structure in a hybrid plasmonic InP-based waveguide. By tuning the graphene’s chemical potential within the 0.4–0.5 eV, we demonstrated the feasibility of an EA-modulator with a length of 1 μm and a bandwidth of

80 GHz. Furthermore, we comprehensively analyzed the SiO<sub>2</sub> guiding and Au layers thicknesses on IL and ER. We showed that a thinner SiO<sub>2</sub> layer exhibits higher optical absorption in the off state (at a chemical potential of 0.525 eV). i.e., for a SiO<sub>2</sub> layer thickness of 10 nm, the optical absorption is six times higher than that of a 50 nm SiO<sub>2</sub> layer due to the closer proximity of the optical field to the graphene layer. Finally, by evaluating the equivalent elements of the proposed EAM, the 3-dB bandwidth of 70 GHz is determined. Moreover, our results demonstrated that increasing the SiO<sub>2</sub> thickness could yield a modulator with a broader bandwidth. The practical applications of optical modulators are extensive and span various domains, underscoring their versatility and significance. These applications include data centers, microprocessors, sensors, advanced medical imaging, and quantum information processing. Optical modulators are indispensable tools in modern technologies due to their ability to modulate light with high speed and precision, contributing to a wide spectrum of applications. In this study, they are examined as integral components of integrated optical circuits, offering potential as data transmission solutions within such circuits. The proposed device is suitable for highly compact integrated photonic circuits, surpassing other modulator configurations in simplicity and complexity. Notably, this study presents the first instance where a graphene-based modulator with a straightforward and extremely short device is proposed on the InP platform.

**Author contributions** HN: Conceptualization, Data curation, Formal analysis, Investigation, Methodology, Software, Writing. MN: Project administration, Resources, Software, Supervision, Validation, Visualization, Writing, Review, Revise & Editing. HS: Advising, Validation, Visualization, Review, Revise & Editing.

**Funding** This research received no specific grant from any funding agency in the public, commercial, or not-for-profit sectors.

**Availability of data and material** The corresponding author's data supporting this study's findings are available upon reasonable request.

## Declarations

**Conflict of interest** The authors declare no conflicts of interest.

**Ethical approval** The authors have completely observed the ethical issues, including plagiarism, informed consent, misconduct, data fabrication and/or falsification, double publication and/or submission, and redundancy.

## References

- Alden Mostaan, S.M., Saghaei, H.: A tunable broadband graphene-based metamaterial absorber in the far-infrared region. *Opt. Quantum Electron.* **53**, 96 (2021). <https://doi.org/10.1007/s11082-021-02744-y>
- Ando, T., Zheng, Y., Suzuura, H.: Dynamical conductivity and zero-mode anomaly in honeycomb lattices. *J. Phys. Soc. Jpn.* **71**, 1318–1324 (2013). <https://doi.org/10.1143/JPSJ.71.1318>
- Ansell, D., Radko, I.P., Han, Z., Rodriguez, F.J., Bozhevolnyi, S.I., Grigorenko, A.N.: Hybrid graphene plasmonic waveguide modulators. *Nat. Commun.* **6**, 2–7 (2015). <https://doi.org/10.1038/ncomms9846>
- Bao, Q., Loh, K.P.: Graphene photonics, plasmonics, and broadband optoelectronic devices. *ACS Nano* **6**, 3677–3694 (2012). <https://doi.org/10.1021/nn300989g>
- Baqir, M.A., Farmani, A., Fatima, T., Raza, M.R., Shaukat, S.F., Mir, A.: Nanoscale, tunable, and highly sensitive biosensor utilizing hyperbolic metamaterials in the near-infrared range. *Appl. Opt.* **57**, 9447–9454 (2018)



- Baqir, M.A., Choudhury, P.K., Farmani, A., Younas, T., Arshad, J., Mir, A., Karimi, S.: Tunable plasmon induced transparency in graphene and hyperbolic metamaterial-based structure. *IEEE Photonics J.* **11**, 1–10 (2019)
- Baqir, M.A., Farmani, A., Raza, M., Akhtar, M.N., Hussain, A.: Engineering of metallic nanorod-based hyperbolic metamaterials for broadband applications operating in the infrared regime. *Appl. Nanosci.* **11**, 229–240 (2021)
- Bijlani, B., Luo, Y., Feng, D., Liao, S., Luff, B.J., Liang, H., Asghari, M., Cunningham, J., Shafiha, R., Fong, J., Krishnamoorthy, A.V.: High speed GeSi electro-absorption modulator at 1550 nm wavelength on SOI waveguide. *Opt. Express* **20**, 22224–22232 (2012). <https://doi.org/10.1364/OE.20.022224>
- Bogaerts, W., Barklund, A., Yu, H., Li, J., Alloatti, L., Korn, D., Palmer, R., Fedeli, J., Wieland, J., Leuthold, J., Dinu, R., Koos, C., Dumon, P., Fournier, M., Freude, W., Baets, R., Hillerkuss, D.: 42.7 Gbit/s electro-optic modulator in silicon technology. *Opt. Express* **19**, 11841–11851 (2011). <https://doi.org/10.1364/OE.19.011841>
- Bonaccorso, F., Sun, Z., Hasan, T., Ferrari, A.C.: Graphene photonics and optoelectronics. *Nat. Photonics* **4**, 611–622 (2010). <https://doi.org/10.1038/nphoton.2010.186>
- Calafell, I.A., Cox, J.D., Radonjić, M., Saavedra, J.R.M., García de Abajo, F.J., Rozema, L.A., Walther, P.: Quantum computing with graphene plasmons. *NPJ Quantum Inf.* **5**, 37 (2019). <https://doi.org/10.1038/s41534-019-0150-2>
- Chen, Z., Appenzeller, J.: Mobility extraction and quantum capacitance impact in high performance graphene field-effect transistor devices (2008)
- Dawlaty, J.M., Shivaraman, S., Strait, J., George, P., Chandrashekar, M., Rana, F., Spencer, M.G., Vekler, D., Chen, Y.: Measurement of the optical absorption spectra of epitaxial graphene from terahertz to visible. *Appl. Phys. Lett.* **93**, 131905 (2008). <https://doi.org/10.1063/1.2990753>
- Dereux, A., Gosciniaik, J., Kjelstrup-Hansen, J., Volkov, V.S., Markey, L., Andersen, T.B., Bozhevolnyi, S.I.: Thermo-optic control of dielectric-loaded plasmonic waveguide components. *Opt. Express* **18**, 1207–1216 (2010). <https://doi.org/10.1364/OE.18.001207>
- Dereux, A., Gosciniaik, J., Markey, L., Bozhevolnyi, S.I.: Efficient thermo-optically controlled Mach-Zehnder interferometers using dielectric-loaded plasmonic waveguides. *Opt. Express* **20**, 16300–16309 (2012). <https://doi.org/10.1364/OE.20.016300>
- Didari-Bader, A., Saghaei, H.: Penrose tiling-inspired graphene-covered multiband terahertz metamaterial absorbers. *Opt. Express* **31**, 12653–12668 (2023)
- Ebbesen, T.W., Genet, C., Bozhevolnyi, S.I.: Surface-plasmon circuitry. *Phys. Today* **61**, 44–50 (2008). <https://doi.org/10.1063/1.2930735>
- Emaminejad, H., Mir, A., Farmani, A.: Design and simulation of a novel tunable terahertz biosensor based on metamaterials for simultaneous monitoring of blood and urine components. *Plasmonics* **16**, 1537–1548 (2021)
- Fan, M., Yang, H., Zheng, P., Hu, G., Yun, B., Cui, Y.: Multilayer graphene electro-absorption optical modulator based on double-stripe silicon nitride waveguide. *Opt. Express* **25**, 21619–21629 (2017). <https://doi.org/10.1364/oe.25.021619>
- Farmani, A., Miri, M., Sheikhi, M.H.: Design of a high extinction ratio tunable graphene on white graphene polarizer. *IEEE Photonics Technol. Lett.* **30**, 153–156 (2017)
- Geim, A.K., Novoselov, K.S.: The rise of graphene. *Nat. Mater.* **6**, 183–191 (2007)
- Giambra, M.A., Soriano, V., Miseikis, V., Marconi, S., Montanaro, A., Galli, P., Pezzini, S., Coletti, C., Romagnoli, M.: High-speed double layer graphene electro-absorption modulator on SOI waveguide. *Opt. Express* **27**, 20145–20155 (2019). <https://doi.org/10.1364/OE.27.020145>
- Giubileo, F., Di Bartolomeo, A.: The role of contact resistance in graphene field-effect devices. *Prog. Surf. Sci.* **92**, 143–175 (2017). <https://doi.org/10.1016/j.progsurf.2017.05.002>
- Gosciniaik, J., Tan, D.T.H.: Theoretical investigation of graphene-based photonic modulators. *Sci. Rep.* **3**, 1–6 (2013a). <https://doi.org/10.1038/srep01897>
- Gosciniaik, J., Tan, D.T.H.: Graphene-based waveguide integrated dielectric-loaded plasmonic electro-absorption modulators. *Nanotechnology* **24**, 185202 (2013b). <https://doi.org/10.1088/0957-4484/24/18/185202>
- Hamzavi-Zarghani, Z., Yahaghi, A., Matekovits, L., Farmani, A.: Tunable mantle cloaking utilizing graphene metasurface for terahertz sensing applications. *Opt. Express* **27**, 34824–34837 (2019)
- Hao, R., Du, W., Chen, H., Jin, X., Yang, L., Li, E.: Ultra-compact optical modulator by graphene induced electro-refraction effect. *Appl. Phys. Lett.* **103**, 061116 (2013). <https://doi.org/10.1063/1.4818457>
- Holmgaard, T., Bozhevolnyi, S.I.: Theoretical analysis of dielectric-loaded surface plasmon-polariton waveguides. *Phys. Rev. B Condens. Matter Mater. Phys.* **75**, 1–12 (2007). <https://doi.org/10.1103/PhysRevB.75.245405>

- Hu, Y., Pantouvaki, M., Van Campenhout, J., Brems, S., Asselberghs, I., Huyghebaert, C., Absil, P., Van Thourhout, D.: Broadband 10 Gb/s operation of graphene electro-absorption modulator on silicon. *Laser Photon Rev.* **10**, 307–316 (2016). <https://doi.org/10.1002/lpor.201500250>
- Huang, H., Chen, S., Wee, A.T.S., Chen, W.: Epitaxial growth of graphene on silicon carbide (SiC). In: *Graphene*, pp. 177–198. Elsevier (2014)
- Khajeh, A., Hamzavi-Zarghani, Z., Yahaghi, A., Farmani, A.: Tunable broadband polarization converters based on coded graphene metasurfaces. *Sci. Rep.* **11**, 1296 (2021)
- Koester, S.J., Li, M.: High-speed waveguide-coupled graphene-on-graphene optical modulators. *Appl. Phys. Lett.* **100**, 171107 (2012). <https://doi.org/10.1063/1.4704663>
- Koester, S.J., Li, M.: Waveguide-coupled graphene optoelectronics. *IEEE J. Sel. Top. Quantum Electron.* **20**, 84–94 (2014). <https://doi.org/10.1109/JSTQE.2013.2272316>
- Koester, S.J., Li, H., Li, M.: Switching energy limits of waveguide-coupled graphene-on-graphene optical modulators. *Opt. Express* **20**, 20330–20341 (2012). <https://doi.org/10.1364/oe.20.020330>
- Lee, B.G., Biberman, A., Chan, J., Bergman, K.: High-performance modulators and switches for silicon photonic networks-on-chip. *IEEE J. Sel. Top. Quantum Electron.* **16**, 6–22 (2010). <https://doi.org/10.1109/JSTQE.2009.2028437>
- Liu, A., Jones, R., Liao, L., Samara-Rubio, D., Rubin, D., Cohen, O., Nicolaescu, R., Paniccia, M.: A high-speed silicon optical modulator based on a metal-oxide-semiconductor capacitor. *Nature* **427**, 615–618 (2004). <https://doi.org/10.1038/nature02310>
- Liu, M., Yin, X., Ulin-Avila, E., Geng, B., Zentgraf, T., Ju, L., Wang, F., Zhang, X.: A graphene-based broadband optical modulator. *Nature* **474**, 64–67 (2011). <https://doi.org/10.1038/nature10067>
- Liu, M., Yin, X., Zhang, X.: Double-layer graphene optical modulator. *Nano Lett.* **12**, 1482–1485 (2012). <https://doi.org/10.1021/nl204202k>
- Lu, Z., Zhao, W.: Nanoscale electro-optic modulators based on graphene-slot waveguides. *J. Opt. Soc. Am. B* **29**, 1490–1496 (2012). <https://doi.org/10.1364/josab.29.001490>
- Naghizade, S., Saghaei, H.: Tunable graphene-on-insulator band-stop filter at the mid-infrared region. *Opt. Quantum Electron.* **52**, 224 (2020). <https://doi.org/10.1007/s11082-020-02350-4>
- Naghizade, S., Saghaei, H.: A tunable electro-optic analog to digital converter using graphene nanoshells in photonic crystal resonators. *JOSA B* **38**, 2127–2134 (2021a)
- Naghizade, S., Saghaei, H.: Ultra-fast tunable optoelectronic half adder/subtractor based on photonic crystal ring resonators covered by graphene nanoshells. *Opt. Quantum Electron.* **53**, 380 (2021b). <https://doi.org/10.1007/s11082-021-03071-y>
- Naghizade, S., Saghaei, H.: Tunable electro-optic analog-to-digital converter using graphene nanoshells in photonic crystal ring resonators. *J. Opt. Soc. Am. B* **38**, 2127–2134 (2021bc). <https://doi.org/10.1364/JOSAB.423088>
- Naghizade, S., Saghaei, H.: Ultra-fast tunable optoelectronic full-adder based on photonic crystal ring resonators covered by graphene nanoshells. *Physica E Low Dimens. Syst. Nanostruct.* **142**, 115293 (2022). <https://doi.org/10.1016/j.physe.2022.115293>
- Naghizade, S., Didari-Bader, A., Saghaei, H.: Ultra-fast tunable optoelectronic 2-to-4 binary decoder using graphene-coated silica rods in photonic crystal ring resonators. *Opt. Quantum Electron.* **54**, 767 (2022). <https://doi.org/10.1007/s11082-022-04157-x>
- Naghizade, S., Didari-Bader, A., Saghaei, H., Etezad, M.: An electro-optic comparator based on photonic crystal ring resonators covered by graphene nanoshells. *Optik* **283**, 170898 (2023)
- Narayanan Mathivanan, S.: Finite element characterisation of graphene-silicon hybrid waveguides. Diss. City, University of London (2019)
- Nayyeri Raad, A., Saghaei, H., Mehrabani, Y.S.: An optical 2-to-4 decoder based on photonic crystal X-shaped resonators covered by graphene shells. *Opt. Quantum Electron.* **55**, 452 (2023). <https://doi.org/10.1007/s11082-023-04727-7>
- Nikoufard, M., Alamouti, M.K., Pourgholi, S.: Multimode interference power-splitter using InP-based deeply etched hybrid plasmonic waveguide. *IEEE Trans. Nanotechnol.* **16**, 477–483 (2017). <https://doi.org/10.1109/TNANO.2017.2688397>
- Novoselov, K.S., Geim, A.K., Morozov, S.V., Jiang, D., Katsnelson, M.I., Grigorieva, I.V., Dubonos, S.V., Firsov, A.A.: Two-dimensional gas of massless Dirac fermions in graphene. *Nature* **438**, 197–200 (2005). <https://doi.org/10.1038/nature04233>
- Peng, S.A., Jin, Z., Ma, P., Zhang, D.Y., Shi, J.Y., Bin Niu, J., Wang, X.Y., Wang, S.Q., Li, M., Liu, X.Y., Ye, T.C., Zhang, Y.H., Chen, Z.Y., Yu, G.H.: The sheet resistance of graphene under contact and its effect on the derived specific contact resistivity. *Carbon* **82**, 500–505 (2015). <https://doi.org/10.1016/j.carbon.2014.11.001>

- Pizzocchero, F., Jessen, B.S., Gammelgaard, L., Andryieuski, A., Whelan, P.R., Shivayogimath, A., Caridad, J.M., Kling, J., Petrone, N., Tang, P.T.: Chemical vapor-deposited graphene on ultraflat copper foils for van der Waals hetero-assembly. *ACS Omega* **7**, 22626–22632 (2022)
- Reed, G.T., Mashanovich, G., Gardes, F.Y., Thomson, D.J.: Silicon optical modulators. *Nat. Photonics* **4**, 518–526 (2010). <https://doi.org/10.1038/nphoton.2010.179>
- Rezaei, M.H., Shiri, M.: High-performance tunable resonant electro-optical modulator based on suspended graphene waveguides. *Opt. Express* **29**, 16299–16311 (2021)
- Rezaei, M.H., Zarifkar, A.: Dielectric-loaded graphene-based plasmonic multilogic gate using a multimode interference splitter. *Appl. Opt.* **57**, 10109–10116 (2018)
- Rezaei, M.H., Zarifkar, A.: High-extinction ratio and ultra-compact two-bit comparators based on graphene-plasmonic waveguides. *Appl. Opt.* **58**, 9829–9838 (2019)
- Rezaei, M.H., Zarifkar, A., Miri, M.: Ultra-compact electro-optical graphene-based plasmonic multi-logic gate with high extinction ratio. *Opt. Mater.* **84**, 572–578 (2018)
- Rezaei, M.H., Zarifkar, A., Miri, M., Alighanbari, A.: Design of a high-efficient and ultra-compact full-adder based on graphene-plasmonic structure. *Superlattices Microstruct.* **129**, 139–145 (2019)
- Rezaei, M.H., Boroumandi, R., Zarifkar, A., Farmani, A.: Nano-scale multifunctional logic gate based on graphene/hexagonal boron nitride plasmonic waveguides. *IET Optoelectron.* **14**, 37–43 (2020)
- Sellathurai, A.J., Mypati, S., Kontopoulou, M., Barz, D.P.J.: High yields of graphene nanoplatelets by liquid phase exfoliation using graphene oxide as a stabilizer. *Chem. Eng. J.* **451**, 138365 (2023)
- Shu, H., Su, Z., Huang, L., Wu, Z., Wang, X., Zhang, Z., Zhou, Z.: Significantly high modulation efficiency of compact graphene modulator based on silicon waveguide. *Sci. Rep.* **8**, 1–8 (2018). <https://doi.org/10.1038/s41598-018-19171-x>
- Sirleto, L., Coppola, G., Iodice, M., Casalino, M., Giofrè, M., Rendina, I.: Thermo-optical switches. In: *Optical Switches: Materials and Design*, pp. 61–96. Woodhead Publishing (2010)
- Smit, M., Williams, K., Van Der Tol, J.: Past, present, and future of InP-based photonic integration. *APL Photonics* **4**, 050901 (2019). <https://doi.org/10.1063/1.5087862>
- Soleimannezhad, F., Nikoufard, M., Mahdian, M.A.: Low-loss indium phosphide-based hybrid plasmonic waveguide. *Microw. Opt. Technol. Lett.* **63**, 2242–2251 (2020). <https://doi.org/10.1002/mop.32488>
- Soref, R.A., Bennett, B.R.: Electrooptical effects in silicon. *IEEE J. Quantum Electron.* **23**, 123–129 (1987). <https://doi.org/10.1109/JQE.1987.1073206>
- Thomson, D.J., Hu, Y., Reed, G.T., Fedeli, J.M.: Low loss MMI couplers for high performance MZI modulators. *IEEE Photonics Technol. Lett.* **22**, 1485–1487 (2010). <https://doi.org/10.1109/LPT.2010.2063018>
- Vakil, A., Engheta, N.: Transformation optics using graphene. *Science* **332**, 1291–1294 (1979). [https://doi.org/10.1126/SCIENCE.1202691/SUPPL\\_FILE/VAKIL-SOM.PDF](https://doi.org/10.1126/SCIENCE.1202691/SUPPL_FILE/VAKIL-SOM.PDF)
- Woehrl, N., Ochedowski, O., Gottlieb, S., Shibasaki, K., Schulz, S.: Plasma-enhanced chemical vapor deposition of graphene on copper substrates. *AIP Adv.* **4**, 047128 (2014)
- Xia, J., Chen, F., Li, J., Tao, N.: Measurement of the quantum capacitance of graphene. *Nat. Nanotechnol.* **4**, 505–509 (2009). <https://doi.org/10.1038/nnano.2009.177>
- Xia, F., Perebeinos, V., Lin, Y.M., Wu, Y., Avouris, P.: The origins and limits of metal-graphene junction resistance. *Nat. Nanotechnol.* **6**, 179–184 (2011). <https://doi.org/10.1038/nnano.2011.6>
- Xu, Q., Schmidt, B., Pradhan, S., Lipson, M.: Micrometre-scale silicon electro-optic modulator. *Nature* **435**, 325–327 (2005). <https://doi.org/10.1038/nature03569>
- Ye, S., Wang, Z., Tang, L., Zhang, Y., Lu, R., Liu, Y.: Electro-absorption optical modulator using dual-graphene-on-graphene configuration. *Opt. Express* **22**, 26173–26180 (2014). <https://doi.org/10.1364/oe.22.026173>

**Publisher's Note** Springer Nature remains neutral with regard to jurisdictional claims in published maps and institutional affiliations.

Springer Nature or its licensor (e.g. a society or other partner) holds exclusive rights to this article under a publishing agreement with the author(s) or other rightsholder(s); author self-archiving of the accepted manuscript version of this article is solely governed by the terms of such publishing agreement and applicable law.